A Finite element model for temperature calculations in absorbing-emitting medium

Rakenteiden Mekaniikka, Vol. 35
Nro 2, 2002, s. 25-35

Djebar Baroudi

ABSTRACT: An implicit temperature calculation algorithm in an absorbing and emitting medium (grey gas) is presented. Emphasis is made on the thermal radiation calculation where the concept of divergence vector of the radiant heat flux vector is used. This allows to treat the thermal radiation as a 'standard' source term in the energy equation. A simplified physical model for computing temperature distribution within the spherical emitting and absorbing region (called *fire ball*, for shortness) is utilized for illustration purposes. The nonlinear transient heat equation is semidiscretised by the finite element method. The time-integration is performed by implicit Backward-Euler method. The radiant transfer equation (RTE) is integrated using the implicit mid-point scheme.

Nomenclature

ω	solid angle, sr
r	radial location, m
$\vec{s}$	unit direction vector defined by the solid angle ω (Fig. 1)
$I(r, \vec{s}(\omega), t)$	radiant intensity at r in direction $\vec{s}$ (Fig. 1), W/m^2.sr
$I_b(r, t)$	black body thermal radiation, W/m^2.sr
$\vec{q}_r(r, t)$	radiant heat flux vector, W/m^2
$Q_r(r, t)$	radiation source term, W/m^3
$Q_{ch}(r, t)$	heat release rate per unit volume, W/m^3

Matrices

$\Theta_{N\times 1}$	temperature global degrees of freedom
$\mathbf{C}_{N\times N}$	capacity matrix
$\mathbf{K}_{N\times N}$	conductivity matrix
$\mathbf{q}_{N\times 1}$	nodal flux column vector

1 Introduction

The temperature distribution inside the absorbing and emitting medium, as schematically shown in Figure 1, is considered. The case of spherical symmetry is treated. The medium can be roughly seen as an idealized flame. But this is an over simplified

approximation, since for instance the convection of hot gases and the soot formation and oxidation, in the flame, are ignored. The main purpose of this paper is to propose an implicit algorithm for heat radiation calculations within the 'flame', to use in conjuction with an implicit finite element formulation of the energy balance equation.

To illustrate the algorithm, the idealised flame is considered. The flame is assumed to be spherical with no dilatation and no convection. These assumtions do not naturally hold for a physical flame. But, for a flame in microgravity [8], the geometrical assumption for the shape is exact. Inside the flame, thermal radiation is emitted and absorbed by the hot gas-soot mixture. This gas-soot mixture which forms the flame, is assumed to behave like a grey gas[1] with no-reflecting boundary. Please, refer to the text book [4] for basics on thermal radiation. Let the hypothetical flame be confined within the sphere of radius R. The outside region of that ball consists of air. The heat release rate per unit volume is non zero in the flame and zero elsewhere (Fig. 1). The heat release rate comes from the exothermic oxidation of the fuel with air oxygen (burning).

2 Mathematical formulation

One of the purposes of this paper is to illustrate the thermal radiation calculation algorithm.

The energy balance over the control volume $\Omega = [0, R_\infty]$ is written as

$$\rho c \frac{\partial T(r,t)}{\partial t} = -\nabla \cdot (-k \nabla T(r,t)) + Q_r(r,t) + Q_{ch}(r,t). \tag{1}$$

In Eq. (1) the internal convective term is ignored. The dilatation of the gas is also ignored. Eq. (1) should be complemented with appropriate initial and boundary conditions. The heat release rate density $Q_{ch}(r,t)$ is assumed to be constant over the flame ($r \in [0, R]$) and zero outside the flame ($r > R$, the ambient air with temperature T_∞ at $r \gg R$). When computing the radiation source (sink) term $Q_r(r,t)$ the concept of divergence vector of the radiant heat flux vector is used; *the net radiant energy density equals that negative divergence* [4]. In other words, in Eq. (1) $Q_r(r,t) \equiv -\nabla \cdot \vec{q}_r(r,t)$ and

$$-\nabla \cdot \vec{q}_r(r,t) = \kappa(T(r,t)) \left(\int_{4\pi} I(r, \vec{s}(\omega), t) \mathrm{d}\omega - 4\pi I_b(r,t) \right). \tag{2}$$

Before entering mathematical details, let us give the thermal radiation algorithm in a verbal form: The divergence of the radiative heat flux is formally similar to the divergence of the conductive heat flux. But now instead of using a simple constitutive law for radiant heat flux as for instance, Fourier law, we now have

[1] this is an approximation where the radiation problem is assumed to be 'independent' of the wavelength.

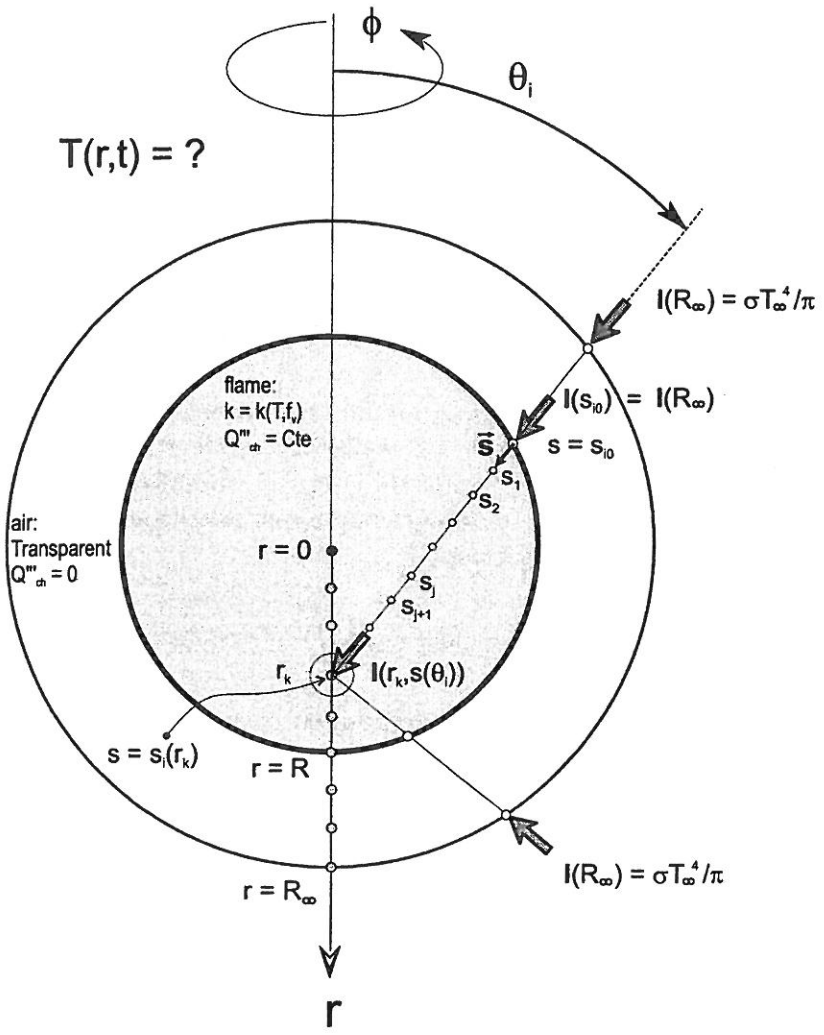

Figure 1: Scheme of the physical problem and its discretization. The 'fire ball', the emitting and absorbing medium, is assumed to have spherical symmetry.

simply more lengthy[2] calculations to perform. One should first, at each location r, integrate the radiant transfer equation (RTE) (Eq. 3) along all directions $\vec{s}(\omega)$ ending at that location to obtain the radiant intensities I at r, needed in Eq. (2), and then use the divergence concept and sum up functions of these intensities and black body radiation all over the solid angles originating from that location to finally obtain the divergence (2) to be directly inserted into (1) as $Q_r(r,t)$.

In the 'fire ball' application, the grey gas assumption is made, *i.e.*, absorbing-emitting grey gas with no scattering. This is justified as the size of soot particles in the flame remains less than 0.1 μm [5, *Thermal radiation section*] which is less

[2]One basic difference being that Fourier law acts only locally at r while the radiation acts at r globally from every spatial point visible to r. This is what makes computations more heavy compared to diffusive flux computations, even when the spectral dependence of the equations is ignored as in the grey gas assumption.

than that thermal radiation wavelength[3]. The Planck mean absorbtion coefficient from the contribution of the soot[4] $\kappa = 11.8 f_v T$ (1/cm) [6], is proportional to the soot volume fraction f_v [9]. The solid angle $\mathrm{d}\omega = \sin\theta \mathrm{d}\theta \mathrm{d}\phi$ and the radiant intensity at location r in the direction of the unit vector $\vec{s}$ is $I(r, \vec{s}(\omega), t)$ (W/m^2.sr). The black body thermal radiation being $I_b(r,t) = \sigma T^4(r,t)/\pi$. The radiant intensity $I(r, \vec{s}(\omega), t)$ at location r along the direction $\vec{s}$, is obtained as $I(s_r(\omega), t)$ by integrating the initial value problem

$$\frac{dI(s,t)}{ds} = \kappa(T(s,t))\,(I_b(s,t) - I(s,t)) \tag{3}$$

along the straight path $s(\omega) \in [s_0,\ s_r(\omega)]$ defined by the direction $\vec{s}$, from a point s_0 with known initial value $I(s_0, t) = I_\infty$ ($s_0 \in \partial\Omega$ where $I_\infty = \sigma T_\infty^4/\pi$) to point $s = s_r(\omega)$. The points $s_r(\omega)$ and r coincide (Fig. 1). Finally, the radiant energy density $U(r,t)$ in (2) is obtained by integrating along all the solid angles $\mathrm{d}\omega$. In a spherically symmetrical case, this gives

$$U(r,t) \equiv \int_{4\pi} I(r, s(\omega), t)\mathrm{d}\omega = 2\pi \int_0^\pi I(r, s(\theta), t) \sin\theta \mathrm{d}\theta \tag{4}$$

The cases where the soot radiation dominates over the gas radiation are now considered. This is true for relatively large soot volume fractions f_v, say $> 10^{-7}$. The mean absorbtion coefficient is $\kappa = 11.8 f_v T$ (1/cm). It is assumed, to illustrate the radiation calculation, that the soot volume fraction f_v is constant [6]. In flames, usually, the soot volume fraction f_v is within the interval 10^{-5}–10^{-7} [5]. In real fire situations, f_v is *a priori* unknown transient field [6] where the soot formation and oxidation should be considered [7]. Generally, there is more soot in the middle than at the 'boundary' of a flame.

3 Numerical formulation

A natural way to solve the energy equation is now to use the finite element (FE) formulation [1]. The classical approximation of the temperature field as

$$T^{(e)}(r,t) = \sum_{i=1}^{N} \phi_i(r) \Theta_i^{(e)}(t) \tag{5}$$

[3]Thermal radiation spectrum range $\approx 0.1 - 100$ μm [5, *Thermal radiation section*] and [9], this length being larger than soot particle dimensions (< 0.1 μm in flame) and therefore no scattering occurs.

[4]Gaseous combustion products are H_2O, CO_2 and soot. The contribution κ_g from these gases (to the mean absorbtion coefficient) should be added in cases where their contributions are of the order of that of soot (with small $f_v < 10^{-7}$). In this case: $\kappa = \kappa_g + \kappa_s$. The absorbsion coefficient of the gases κ_g should be included: Planck mean absorbtion coefficient for various gases as function of T are reported in [5, Thermal radiation section: 1-73, Fig. 1-4.7] from which κ_g can be obtained. (this should be added to κ_s). For soot [5, Eq. (39)] gives a mean absorbtion coefficient κ_s.

is made, where the basis functions $\phi_i(r)$ are the standard linear piecewise functions over the element e defined over $r \in [r_1^{(e)}, r_2^{(e)}]$, $e = 1 \ldots N_e$ and $\Theta_i^{(e)}(t)$ being the nodal temperatures of the element. Inserting this approximation into the weak form of (1) and using the Galerkin method, one obtains the semidiscrete energy balance equations [1], [2]

$$\mathbf{C}^{(k-1)} \cdot \frac{\mathrm{d}\boldsymbol{\Theta}^{(k)}}{\mathrm{d}t} = -\mathbf{K}^{(k-1)} \cdot \boldsymbol{\Theta}^{(k)} + \mathbf{q}^{(k-1)} + \mathbf{q}_{ch}{}^{(k-1)} + \mathbf{q}_r{}^{(k-1)}. \tag{6}$$

The matrices and column vectors in (6), excluding the capacty matrix, are calculated by Gauss quadrature using one integration point. The capacity matrix is calculated using the Newton-Cotes scheme to obtain a diagonal matrix $\mathbf{C}$. The term $\mathbf{q}(t)$ contains the boundary conditions. The term $\mathbf{q}_{ch}(t)$ includes the heat release rate generated by the burning of the fuel. The time-integration of the resulting system of nonlinear ordinary differential equations (6) is performed with the implicit backward-Euler (BE) method [1] with the algorithm

$$\boldsymbol{\Theta}_n^{(k+1)} = \boldsymbol{\Theta}_{n-1} + \Delta\boldsymbol{\Theta}_n^{(k)}, \tag{7}$$

where $\Delta\boldsymbol{\Theta}_n^{(k)}$ is solution of

$$\mathbf{C}_n^{(k)} \cdot \Delta\boldsymbol{\Theta}_n^{(k)} = \Delta\mathbf{q}_n^{(k)}, \tag{8}$$

with

$$\Delta\mathbf{q}_n^{(k)} = \left(-\mathbf{K}_n^{(k)} \cdot \boldsymbol{\Theta}_n^{(k)} + \mathbf{q}_n^{(k)} + (\mathbf{q}_{ch})_n^{(k)} + (\mathbf{q}_r)_n^{(k)}\right) \cdot \Delta t_n. \tag{9}$$

In (8) the column vector $\Delta\boldsymbol{\Theta}_n^{(k)}$ is solved using the Gaussian elimination scheme. The time step $\Delta t_n = t_{n+1} - t_n$. When solving Eqs. (7)–(9), the Picard iteration scheme is used. The convergence (stopping) criteria for the iteration step $k+1$ is $\|T^{k+1} - T^k\|/\|T^{k+1}\| \leq RTOL$ at each t_n, with $RTOL = 10^{-3}$ used with the definition $\|T\|^2 = \int_0^{R_\infty} |T(r, t_n)|^2 \mathrm{d}r$. The matrices and column vectors are detailed in Appendix (A).

3.1 Calculation of the radiative source term

The source term $Q_r(r_k, t) \equiv -\nabla \cdot \vec{q}_r(r_k, t)$ is computed by numerically integrating Eq. (2) at locations $r_k \in [0, R]$, where $k = 1 \ldots N_e + 1$ being the nodal points on r. The numerical quadrature is performed in the next way: First the angle θ is discretised into N_θ angles θ_i ($i = 1 \ldots N_\theta$ and $\Delta\theta_j = \theta_{j+1} - \theta_j$) such that $\sin\theta_i \Delta\theta_i$ is constant[5]. Then, the IVP (3) is numerically integrated, using the implicit midpoint scheme ($O(\Delta s)^2$) [3], along the straight path $s(\theta_i) \in [s_{i0},\ s_{ik}]$ to finally obtain $I(r_k, s(\theta_i), t)$ in (4), for $i = 1 \ldots N_\theta$ (Fig. 1). The integration path is the segment starting at the point $s(\theta_i) = s_{i0}$ (on the perimeter $\partial\Omega$ of radius R) and ending at the

[5]to ensure that equal solid angles are obtained, to 'optimize' the accuracy of the numerical quadrature of (4) in case of constant radiant flux. These are recursively solved from $\theta_i - 2/(N_\theta \sin\theta_i) - \theta_{i-1} = 0$, where $\theta_1 = 0$ and $i = 1 \ldots N_\theta - 1$.

point s_{ik} which coincides with r_k. The path $s(\theta_i)$ is discretized into N_s subintervals. The integral (4) is obtained using the trapezoidal rule. By inserting the numerical value of that integral into (2), the radiative source (sink) term $Q_r(r_k, t)$ is finally obtained. Note that $Q_r(r_j, t) = 0$, outside the flame $r_j > R$.

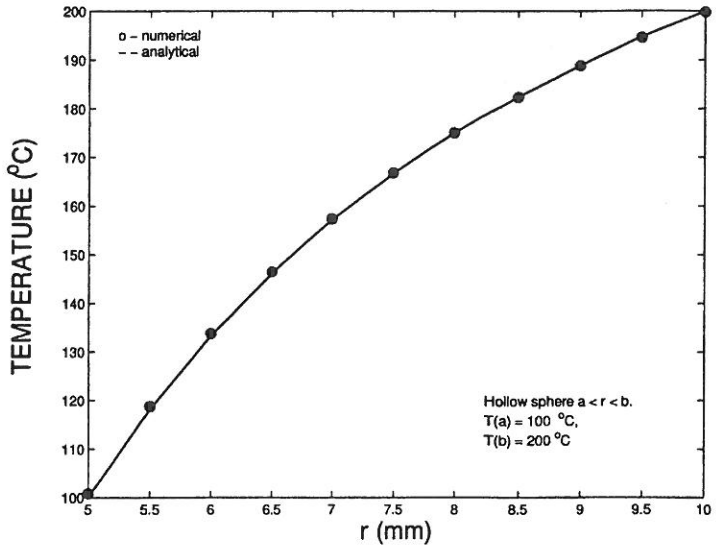

Figure 2: Analytical *versus* numerical solutions. Analytical from Carslaw and Jaeger. Steady case [10, Chap. X, ex. I, p. 231, Eq. (3)]

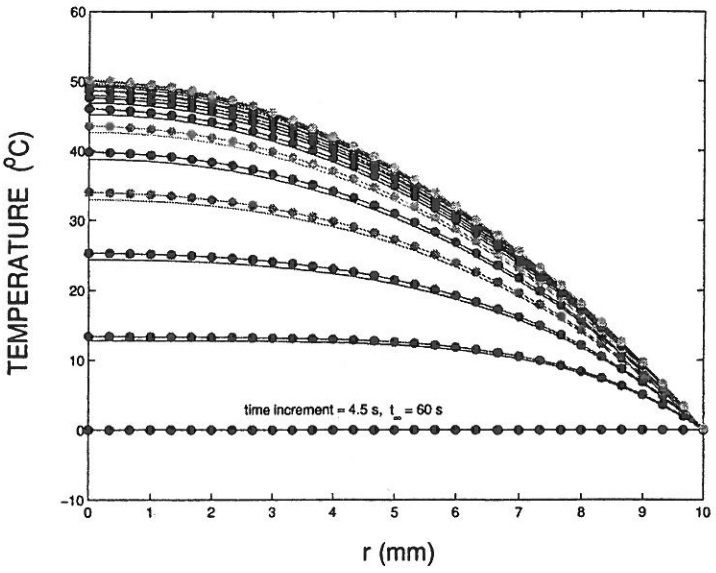

Figure 3: Analytical *versus* numerical solutions. Analytical from Carslaw et al. Transient case. [10, I, p. 243 (Eq. (6))]. The time steps, in the curves, is 4.5 s. The first curve corresponds to intial time 0 s and the last one to 60 s.

4 Numerical examples

4.1 Thermal diffusion only

The implemented numerical solution scheme (without the radiation term) is checked with two known solutions from Carslaw and Jaeger [10]. Two axisymmetric analytical problems: *a) steady solution without source term*: A hollow sphere $a \leq r \leq b$, $T(a) = 100$ °C and $T(b) = 200$ °C , where a and b are 5 and 10 mm, respectively. *b) unsteady case with constant heat source*: A homogenious sphere of 10 mm radius and constant heat generation rate per unit volume of 0.3 MW/m^3 having zero initial and surface temperature. The thermophysical properties used are $\rho = 146$ kg/m^3, $c_p = 800$ J/kg.K and $K = 0.1$ W/m.K. The analytical solutions for the two cases are given in [10, Chap. X, ex. I, p. 231, Eq. (3) and ex. I, p. 243, Eq. (6)]. In both cases the numerical solutions converged to the analytical ones (Figures 2 and 3).

4.2 Flame temperatures including radiation

Transient temperature profiles for a spherical flame with constant input heat release rate density[6] of 1 MW/m^3 are now calculated with the raditative model included. The case of a spherical flame is considered. Temperature dependent thermal properties of air are used for the flame. Results for different absorbtion coefficients are shown in Fig. 4. Results for constant κ_s and for different flame radius are reported in Fig. 5. Note that, the more sooty the flame is (with increasing of soot volume fraction f_v) the colder the flame gets. The visible[7] flame, as seen by a human eye, is due in fact to the radiative heat from the hot soot particles (particle size < 10 nm in flame).

Note that, even in the spherical case with no motion[8] considered here, the calculated temperature profiles do not correspond necessarily to real temperatures, in the sense that in a real flame, the soot volume fraction f_v is an unknown transient field with range 10^{-5}–10^{-7}, and that f_v (as can be seen in Fig. 4) affects significantly the temperatures. However, the calculated temperatures are consistent and fall into the range of observed flame temperatures because the used values for the soot fractions are in observed ranges. But, to calculate the transient flame temperatures more confidently, it is necessary to model adequately the soot formation and oxidation processes to achieve a better description of the radiative heat transfer process.

5 Concluding remarks

An implicit thermal radiation algorithm for integrating the RTE, when solving the energy equation by FEM, is derived. The concept of divergence of the flux vector

[6] the total heat power contained in 1 m^3 of flame is approximately 0.5 – 1 MW/m^3.

[7] visible colours of hot objects: 500°C –first visible red glow, 700°C –Dull red, 900°C –Cherry red, 1100°C –Orange, 1400°C –White [9].

[8] in other words, only heat diffusion and radiation are the heat transfer modes considered.

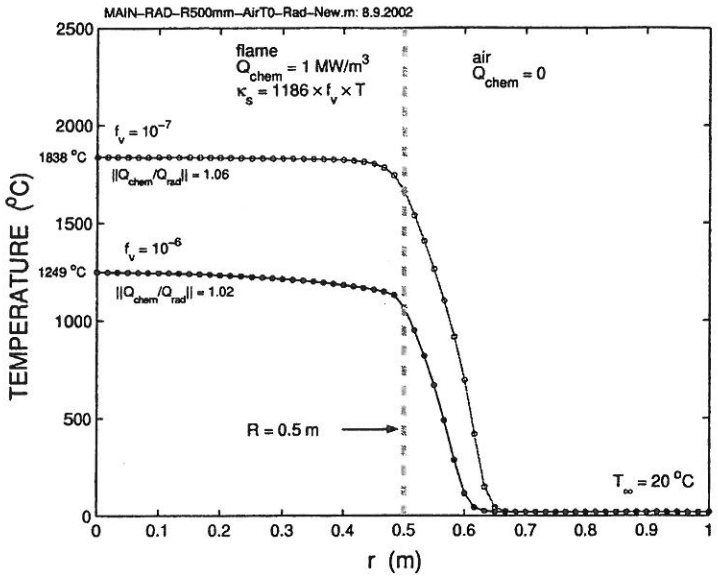

Figure 4: Computed steady temperature distribution in the flame and outside it for $R = 0.5$ m. (grey gas assumption, $\kappa_s = 1186 f_v T$, $f_v = 10^{-6}$ and $f_v = 10^{-7}$ with $Q_{ch} = 1$ MW/m^3).

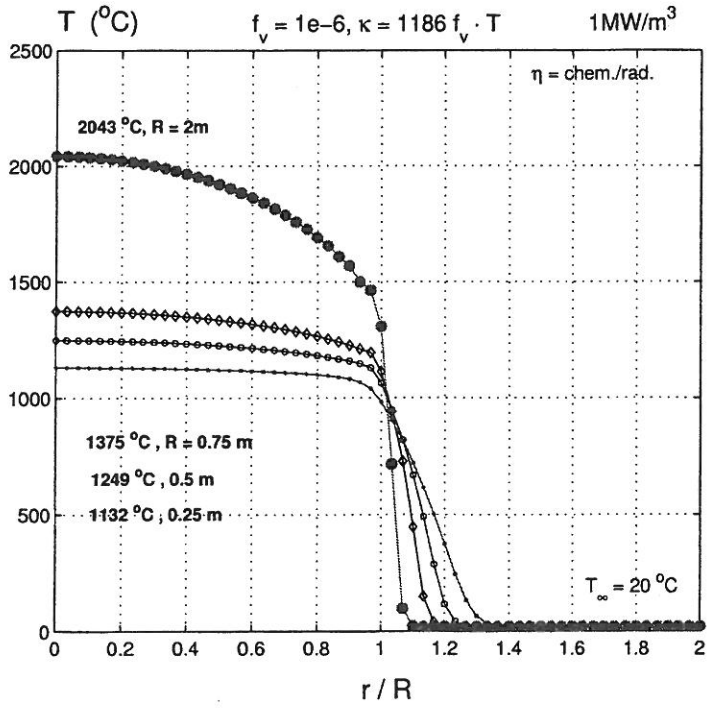

Figure 5: Computed steady temperature distribution in the flame and outside it for $R = 0.25, 0.5, 0.75$ and 2 m. (grey gas assumption, $\kappa_s = 1186 f_v T$ and $f_v = 10^{-6}$ with $Q_{ch} = 1$ MW/m^3).

allows a systematical treatment of the radiation term as a standard heat source (sink) term in the FE-formulation.

Aknowlegments This article is inspired by a simplified problem kindly proposed by Dr. Jukka Vaari (who deserves thanks for that) from the Fire Research group of VTT Building and Transport. Thanks also to Professor Juha Paavola, from the structural mechanics laboratory of HUT, for commenting the manuscript.

A Appendix: Matrices and column vectors

The elementary matrices are

$$C_{ij}^{(e)}(t) = 4\pi \int_{r_1^{(e)}}^{r_2^{(e)}} \rho(T(r,t))c(T(r,t))\,\phi_i(r)\phi_j(r)\,r^2\mathrm{d}r, \tag{10}$$

$$K_{ij}^{(e)}(t) = 4\pi \int_{r_1^{(e)}}^{r_2^{(e)}} k(T(r,t))\,\phi_{i,r}(r)\phi_{j,r}(r)\,r^2\mathrm{d}r, \tag{11}$$

$$(q_r)_i^{(e)}(t) = 4\pi \int_{r_1^{(e)}}^{r_2^{(e)}} (-\nabla\cdot\vec{q}_r(r,t))\,\phi_j(r)\,r^2\mathrm{d}r, \tag{12}$$

$$(q_{ch})_i^{(e)}(t) = 4\pi \int_{r_1^{(e)}}^{r_2^{(e)}} Q_{ch}(r,t)\,\phi_j(r)\,r^2\mathrm{d}r, \tag{13}$$

where $i,j = 1,2$ and $e = 1\ldots N_e$. Assembling of the global matrices (from elementary contributions (10–13)) in (6) is made using standard FE-assembling methods [1]. Matrices (11–13)) are evaluated by Gauss quadrature using one integration point located at the center of the element e. The first term $C_{11}^{(1)}$ is integrated with the scheme $C_{11}^{(1)} = 4\pi(r_1/4)^2\rho(T(r_1/4),t)\,c(T(r_1/4),t)\,(r_2^{(1)}-r_1^{(1)})/2$ to avoid singularity in $\mathbf{C}^{-1} = 1/\mathrm{diag}(\mathbf{C})$ (one Gauss-point at $r_1/4$). For the remaining terms in matrices $C_{ij}^{(e)}$, the Newton-Cotes scheme is used to obtain diagonal matrix $\mathbf{C}$. The nodal flux column vector at the boundary $r \to R_\infty \gg R$ where the ambient air temperature is T_∞ and $I_\infty = \sigma T_\infty^4/\pi$ (with $h \to \infty$, constraint by penalty method)

$$\mathbf{q}_{N\times 1}(t) = 4\pi R_\infty^2 \begin{pmatrix} 0 \\ 0 \\ 0 \\ \vdots \\ 0 \\ 1 \end{pmatrix} \cdot h_\infty\,(T(R_\infty,t) - T_\infty) \qquad . \tag{14}$$

The elementary shape functions, defined on element e, are

$$\phi_1(r) = \frac{r - r_1^{(e)}}{r_2^{(e)} - r_1^{(e)}} \quad \text{and} \quad \phi_2(\mathrm{r}) = 1 - \frac{\mathrm{r} - \mathrm{r}_1^{(e)}}{\mathrm{r}_2^{(e)} - \mathrm{r}_1^{(e)}}, \quad \text{where r} \in [\mathrm{r}_1^{(e)}, \mathrm{r}_2^{(e)}]. \tag{15}$$

References

[1] Zienkiewicz, O. C., *The Finite Element Method*, 3rd Edition. McGraw-Hill. London, 1986, 787 p.

[2] Thomas J. R. Hughes, *The finite element method, linear static and dynamic finite element analysis.* Prentice-Hall International Inc., 1987, 803 p.

[3] K. Eriksson, D. Estep, P. Hansbo, C. Johnson, *Computational differential equations.* Studentlitteratur, 1996, 538 p.

[4] Roberts Siegel and John R. Howell *Thermal radiation heat transfer.*

[5] *SFPE Handbook of Fire Protection Engineering*, 2.nd Ed.

[6] Atreya, A., and Agrawal, S., "Effect of radiative heat loss on diffusion flames in quiescent microgravity atmosphere". *COMBUSTION AND FLAME*, **115** (1998) 372–382.

[7] Makhviladze G. M., Roberts J. P. and Yakush S. E. "Combustion of two-phase hydrocarbon fuel clouds released into the atmosphere." *COMBUSTION AND FLAME*, **118** (1999) 583–605.

[8] Sunderland P. B., Axelbaum R. L., Urban D. L., Chao B. H. and Liu S. "Effects of structure and hydrodynamics on the sooting behavior of spherical microgravity diffusion flames". *COMBUSTION AND FLAME*, **132** (2003) (article in press).

[9] Drysdale, D., *An introduction to FIRE DYNAMICS*, 2nd Edition. John Wiley & Sons. UK, Chichester, 1998, 451 p.

[10] H. S. Carslaw and J. C. Jaeger. *Conduction of heat in solids.* 2nd Ed., Oxford 1959, Oxford University Press.

Djebar Baroudi, MSc. Tech.
Research Scientist
Helsinki University of Technology
Laboratory of Structural Mechanics